PAPER

Bioresponsive polymer coated drug nanorods for breast cancer treatment

To cite this article: Tunyaboon Laemthong *et al* 2017 *Nanotechnology* **28** 045601

View the article online for updates and enhancements.

Bioresponsive polymer coated drug nanorods for breast cancer treatment

Tunyaboon Laemthong[1], Hannah H Kim[2], Kelly Dunlap[1], Caitlin Brocker[1], Dipak Barua[1], Daniel Forciniti[1], Yue-Wern Huang[2] and Sutapa Barua[1]

[1] Department of Chemical and Biochemical Engineering, Missouri University of Science and Technology, Rolla, MO 65409, USA
[2] Department of Biological Sciences, Missouri University of Science and Technology, Rolla, MO 65409, USA

E-mail: baruas@mst.edu

CrossMark

Abstract

Ineffective drug release at the target site is among the top challenges for cancer treatment. This reflects the facts that interaction with the physiological condition can denature active ingredients of drugs, and low delivery to the disease microenvironment leads to poor therapeutic outcomes. We hypothesize that depositing a thin layer of bioresponsive polymer on the surface of drug nanoparticles would not only protect drugs from degradation but also allow the release of drugs at the target site. Here, we report a one-step process to prepare bioresponsive polymer coated drug nanorods (NRs) from liquid precursors using the solvent diffusion method. A thin layer (10.3 ± 1.4 nm) of poly(ε-caprolactone) (PCL) polymer coating was deposited on the surface of camptothecin (CPT) anti-cancer drug NRs. The mean size of PCL-coated CPT NRs was 500.9 ± 91.3 nm length $\times$ 122.7 ± 10.1 nm width. The PCL polymer coating was biodegradable at acidic pH 6 as determined by Fourier transform infrared spectroscopy. CPT drugs were released up to 51.5% when PCL coating dissolved into non-toxic carboxyl and hydroxyl groups. Trastuzumab (TTZ), a humanized IgG monoclonal antibody, was conjugated to the NR surface for breast cancer cell targeting. Combination treatments using CPT and TTZ decreased the HER-2 positive BT-474 breast cancer cell growth by $66.9 \pm 5.3\%$ *in vitro*. These results suggest effective combination treatments of breast cancer cells using bioresponsive polymer coated drug delivery.

S Online supplementary data available from stacks.iop.org/NANO/28/045601/mmedia

Keywords: drug delivery, cancer therapy, nanorods, camptothecin, trastuzumab, polycaprolactone

(Some figures may appear in colour only in the online journal)

Introduction

Protection of molecular structures of drugs is required in order to retain their active groups and therapeutic efficiency. For example, the lactone ring of camptothecin (CPT) drugs is converted to carboxylate form, which possesses high affinity to human serum albumin (HSA) at physiological pH 7.4, and is preferentially eliminated from the body [1, 2] Encapsulation of CPT inside polymer nanoparticles prevents the conversion of CPT into the inactive carboxylate form during blood circulation, thus increasing its likelihood of reaching the target site [3–6]. CPT has been conjugated with a variety of polymers such as β-cyclodextrin [7, 8], N-hydropropylmethacrylamide (HPMA) [9], polylactide (PLA) [10], polyethylene glycol (PEG) and polymethcryloyloxyethyl phosphoroylcholine (polyMPC) [11], to improve efficacy. There are other formulations such as liposomes consisting of floxuridine and CPT-analog irinotecan [12], and micelles comprising of CPT derivative SN38 [13]. The nanostructured derivatives of CPT increase systemic exposure to CPT and

anti-cancer activity in patients; however, the side effects are diarrhea, hepatic toxicity and renal failure [14, 15]. In addition, most nanoparticle–drug conjugates suffer from aggregation with hydrophilic and hydrophobic backbone of nanoparticles [16], and, therefore, low drug release.

In contrast, in the present work, we have developed a method to coat a bioresponsive polymer on elongated drug NRs. While conventional nanoparticles are made of lipids, metals, and polymers, we prepared rod-shape nanoparticles using pure anti-cancer drugs and deposited a thin layer (10.3 ± 1.4 nm) of bioresponsive polymer coating on drug NRs. Recent studies have shown that NRs enhance drug delivery as reflected in improved blood circulation time [17], specific receptor binding [18] and cellular internalization by target cells [18]. Theoretical models and *in vivo* biodistribution studies support these experimental outcomes [17, 19, 20]. Cationic cross-linked PEG hydrogel NRs are internalized by HeLa cells more rapidly than symmetrical shaped particles [21]. Mesoporous silica NRs of 450 nm length are taken up more rapidly than 250 nm rods or 100 nm spherical particles by A375 human melanoma cells [22]. Rod-shaped particles can avoid phagocytosis depending on the initial contact angle to the macrophages [23]. The adhesion strength of non-spherical particles towards the blood vessel wall is higher than spherical nanoparticles, as shown in both experimental setting, and theoretical modeling [19, 24–28]. Accordingly, we prepared drug NRs in this work. We used the solvent diffusion method to prepare CPT NRs of $500.9 \pm 91.3 \times 122.7 \pm 10.1$ nm size in large quantities [29].

We encapsulate CPT drug NRs with a bioresponsive polymer, PCL. This polymer is a US FDA-approved biodegradable aliphatic polyester, and is well-known for hydrolytic cleavage of ester groups, and its non-toxicity [30]. Nanoparticles composed of PCL polymer have been shown to exhibit increased blood circulation time, and reduced clearance by the reticuloendothelial system (RES) [31]. PCL microspheres loaded with bovine serum albumin (BSA) protein released up to 60.5% of BSA *in vitro* [32]. CPT, doxorubicin, and taxol-loaded PCL microspheres efficiently released the loaded drugs from microspheres that resulted in a higher degree of cancer cell growth inhibition than free drugs [33–35]. One drawback of these polymer–drug conjugates is drug's aggregation with polymers [16], and, therefore, low drug release. To overcome these issues, we introduce a simple and rapid technique of interfacial polymer deposition on the surface of pure drug NRs in large quantities. NRs provide greater contact surface area than conventional nanospheres, and thus, ensure greater receptor-ligand interactions for binding [36]. We deposit a PCL coating from liquid precursors surrounding CPT NRs simultaneously during NR formation.

Our nanocarrier system aims at breast cancer cell targeting by human epidermal growth factor 2 (HER-2) protein specific antibody conjugation. TTZ (Herceptin; Genentech) monoclonal antibody (mAb) binds to HER-2 overexpressed at the cell membrane by many cancer cells, including breast cancer cells [37]. It is shown that TTZ-conjugated polystyrene NRs accumulate only in HER-2 positive breast cancer cells by multivalent interactions with HER-2 receptors [18]. TTZ reduces proliferation of breast cancer cells by binding to the extracellular domain of HER-2 receptors, preventing HER-2 dimerization, and thereby inducing subsequent cell cycle arrest in G1 [38]. In this study, we simultaneously delivered CPT and TTZ drugs using PCL coated NRs to achieve synergistic inhibition effects on breast cancer cell growth at low concentrations.

Materials and methods

Synthesis of PCL polymer coated CPT NRs

All reagents were purchased from Sigma-Aldrich (St. Louis, MO, USA) unless otherwise specified. We deposited a thin layer of PCL polymer (14 000 Da) film on CPT NRs using the solvent diffusion method [29]. Briefly, 1 ml each of 10 mg ml^{-1} of CPT in dimethyl sulfoxide (DMSO) and 1 mg ml^{-1} of PCL polymer in toluene were added to a 20 ml of reverse osmosis (RO) water using a syringe pump. Residual toluene was removed by stirring (300 rpm) the CPT–PCL NR suspension overnight at room temperature (RT; $\sim$22 °C). DMSO was removed by centrifugation at 3000 rcf, followed by five times washing using RO water. PCL-coated CPT (CPT–PCL) NRs were freeze-dried, weighed and stored at 4 °C. CPT concentrations were measured and quantified by reading absorbance at 366 nm using a plate reader (BioTek Synergy; BioTek, Winooski, VT, USA), and the CPT calibration curve [18, 29] The theoretical content of PCL weight in CPT–PCL NRs was calculated based on the weight of freeze-dried particles and CPT amount. Percent encapsulation efficiency of CPT and PCL were calculated based on their initial mass of samples.

Characterization of CPT–PCL NRs

The morphology and size of CPT–PCL NRs were examined under transmission electron microscope (TEM; Tecnai F20, Hillsboro, OR, USA) at an accelerating voltage of 120 kV. A drop of 10 μl CPT–PCL solutions in water was air-dried on carbon-coated copper grids (Ted Pella, Redding, CA, USA). The NR diameter, NR length, and thickness of the polymer coating were measured using ImageJ (version 1.45S, NIH, USA). Uncoated CPT NRs were imaged using a scanning electron microscope (SEM; Helios Nanolab 600 FIB, Hillsboro, OR, USA). The surface charges of NRs in PBS were determined by dynamic light scattering using a NanoSeries Zetasizer ZS 90 (Malvern Instruments Ltd, Malvern, Worcestershire, UK), and the backscattering detection at 90°. The zeta potential was measured for 15 runs. Data was analyzed using means and standard deviations of three concentrations.

Degradation of PCL coating and stability of lactone form of CPT in CPT–PCL NRs

The degradation of PCL coating and conversion between lactone and carboxylates in CPT were analyzed by Fourier

transform infrared (FT-IR) spectroscopy. The disappearance of ester groups in PCL backbone and appearance of carboxyl and hydroxyl groups were studied using FT-IR spectra. Briefly, CPT–PCL NRs were incubated for 72 h at 37 °C in PBS at pH 6. Samples were freeze-dried to sublimate any water, and ground at 1:100 weight ratio with FT-IR grade potassium bromide (KBr; Alpha Aesar, Ward Hill, MA, USA). Hydrolytic degradation was monitored by comparing the intensity of ester, alcohol and carboxyl bands at $t = 0$ and 72 h for the same amount of PCL in NRs. To evaluate the conversion of active lactone rings into inactive carboxylic acids in coated NRs, CPT NRs alone without PCL coating was used as a control. The FT-IR absorbance spectra were obtained for 32 scans over the range of 4000–500 cm^{-1} using a Thermo Nicolet Nexus 470 FT-IR (Thermo Electron Corporation, Waltham, MA, USA). The FT-IR spectrometer was equipped with an electronic temperature control (ETC) EverGlo IR Source, and a deuterated triglycine sulfate detector. The sample resolution was set at 4 cm^{-1}. Background noises were obtained from the ambient air without a sample in place and subtracted from the sample spectra. All spectra were analyzed using EZ OMNIC E.S.P v.5.1 software (Thermo Scientific, Waltham, MA, USA).

Quantification of CPT drug release

CPT drug release was conducted by exposing CPT–PCL NRs to phosphate buffered saline (PBS) at pH 6.0 (to mimic the cancer microenvironment) and pH 7.4, and at 37 °C. Bare CPT NRs without the PCL coating was used as a control. PBS of 500 μl were sampled at different time intervals of $t = 0$, 0.5, 2, 4, 8, 24, 36 and 72 h. CPT drug concentrations, that were released to the buffer, were measured using absorbance at 366 nm and CPT standard curve. These test tube experiments were not run in presence of fetal bovine serum (FBS) because FBS has high spectroscopic background noises.

Conjugation of antibody on the surface of CPT–PCL NRs

TTZ antibody (Genentech, South San Francisco, CA, USA) was conjugated to the surface of CPT–PCL NRs by coupling primary amines of TTZ with ester groups of PCL forming amide bonds. Briefly, 10 mg ml^{-1} TTZ solution was prepared in PBS of pH 7.4. 10 mg CPT–PCL NRs were added to 1 ml of TTZ solution, mixed, and incubated at RT. The unreacted reagents were separated using 100 kDa membrane filters (EMD Millipore Amicon Ultra-0.5). The supernatants were collected by centrifugation at 1000 rcf and analyzed by the BCA protein assay (Pierce Biotechnology, Rockford, IL, USA). BSA was used to prepare HER-2 non-targeted CPT–PCL–BSA NRs.

In vitro cell growth inhibition

The effectiveness of combination treatments using CPT–PCL–TTZ NRs was evaluated in HER-2 positive BT-474 breast cancer cells (ATCC) and HER-2 negative cell line MDA-MB-231 (ATCC, Manassas, VA, USA). The cells were cultured in Hybri-Care (ATCC), and RPMI 1640 (Life Technologies, Carlsbad, CA, USA), respectively supplemented with 10% FBS (Corning Inc., Corning, NY, USA) and 1% (100 units ml^{-1}) Penicillin-Streptomycin (Gibco, Carlsbad, CA, USA) at 37 °C and 5% CO$_2$. Cells were plated in 96-well tissue culture plates (Corning) at a density of 10 000 cells/well in 200 μl respective medium. After 18 h of growth, 10 μl of NRs were added to the medium. The final concentrations of CPT were 0.1, 0.2, 0.5, 1, 2, 5 and 10 μg ml^{-1}. The corresponding PCL concentrations were 0.008, 0.017, 0.042, 0.083, 0.167, 0.417 and 0.833 μg ml^{-1}, respectively, and TTZ concentrations were 0.075, 0.15, 0.375, 0.75, 1.5, 3.75 and 7.5 μg ml^{-1}, respectively. CPT–PCL–BSA was used an HER-2 non-specific control. Cells were also treated with the same concentrations of PCL, CPT NR, and TTZ solutions to determine the individual cytotoxic effect. Cells treated with 10 μl of PBS were used as positive controls. The medium was replaced with fresh medium after 3 h. Following 72 h, the plates were centrifuged at 100 rcf for 15 min. The supernatant was discarded. Live cells were stained with 2 μM calcein AM (Life technologies) in PBS by incubating at RT. for 30 min. The fluorescence intensity (F.I.) of calcein AM was measured using 485/528 excitation/emission filters using the plate reader (BioTek Synergy 2). The percentage inhibition of cell growth was calculated using equation (1):

$$\% \text{ inhibition of cell growth}$$
$$= \frac{\text{F.I.}_\text{PBS treated cells} - \text{F.I.}_\text{samples}}{\text{F.I.}_\text{PBS treated cells}} \times 100. \quad (1)$$

To determine the synergistic effects of CPT and TTZ in CPT–PCL–TTZ NRs, a combination index (CI) was calculated based on their individual doses that had equivalent effects, according to the Chou–Talalay method [39, 40]:

$$\text{C. I.} = \left(\frac{[\text{CPT}] \text{ in CPT} - \text{PCL} - \text{TTZ NRs}}{[\text{CPT}] \text{NR alone}} \right)$$
$$+ \left(\frac{[\text{TTZ}] \text{ in CPT} - \text{PCL} - \text{TTZ NRs}}{[\text{TTZ}] \text{ alone}} \right). \quad (2)$$

To examine that the cell growth inhibitory effects were induced by NRs intracellularly, BT-474 cells were incubated with CPT–PCL–TTZ NRs for 6 h at 37 °C in eight-well glass chambers (Lab-Tek). TTZ was labeled with Alex Fluor 594 dye according to the manufacturer (Molecular Probes)'s protocol. After 2 h of NR incubation, the cells were washed with PBS three times to remove unbound particles and re-incubated with the medium for 4 h. Cells were imaged using a scanning laser inverted confocal microscope (Ti-Eclipse; Nikon Inc., Melville, NY, USA) and 40x objective. The excitation/emission used for CPT and Alexa Fluor 594 were 360/400 and 590/617 nm, respectively.

Statistical analysis

Each experiment was carried out with three independent experiments of at least triplicate measurements. The mean differences and standard deviations were evaluated.
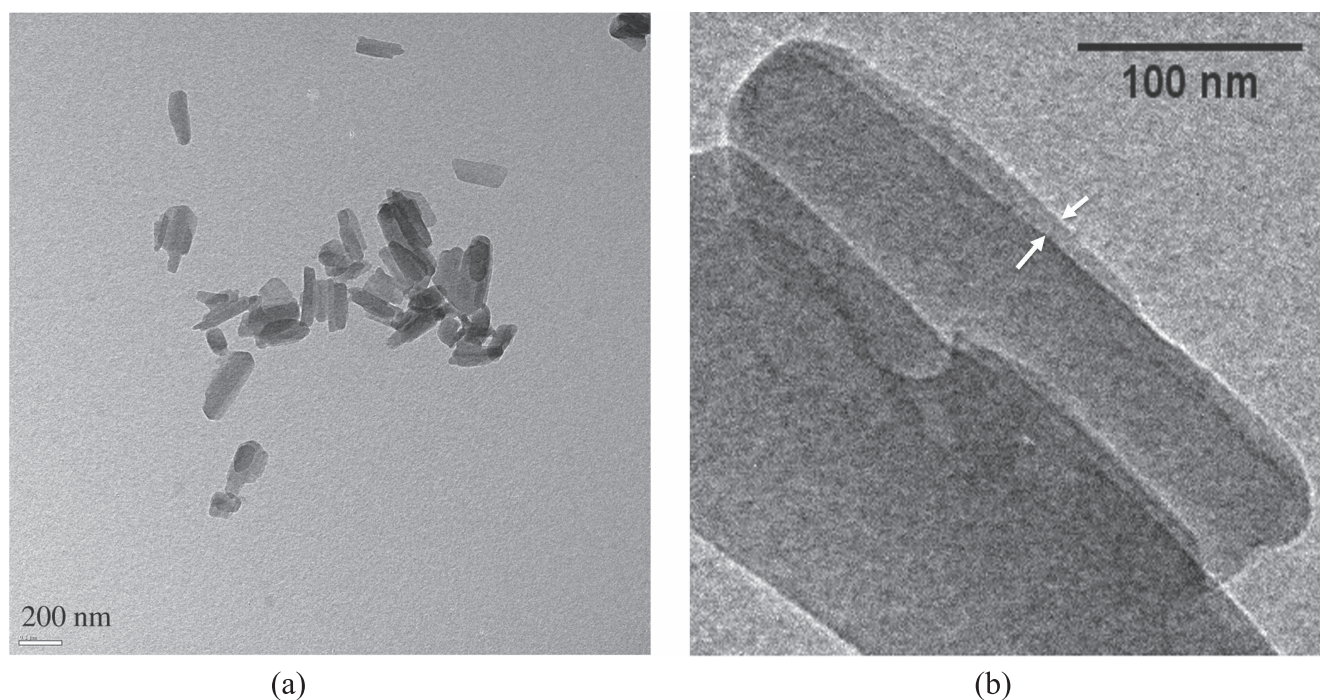
(a)   (b)

Figure 1. TEM images of CPT–PCL NRs. (a) Image showing a homogeneous distribution of CPT–PCL NRs. (b) Magnified view of a thin (~10 nm; arrows) PCL polymer film on CPT NRs.

Results

Preparation of a thin layer of PCL coating on CPT NRs

We developed an engineering technique based on the solvent diffusion method to prepare PCL coated CPT NRs of 500.9 ± 91.3 nm $\times$ 122.7 ± 10.1 nm in length and width, respectively (figure 1(a)). This process involved three steps: phase separation, CPT NR formation, and PCL deposition. CPT NRs were formed because of phase separation from the DMSO oil phase into water under mild stirring ($\sim$300 rpm) [18, 29]. At the same time, PCL polymer films were coated on CPT NRs by virtue of van der Waals attractive forces between CPT NR surface and PCL polymer under low shear stress [41]. The combination of adhesive and shear forces spread the polymer thinly over CPT NRs. A thin layer of 10.3 ± 1.4 nm PCL coating was formed surrounding the CPT NR (figure 1(b). This is a *soft* coating technique that does not require high mechanical agitation, sonication or vibration, thus preventing any structural damage of drugs. In contrast, bare CPT NRs showed no evidence of coating (online supplementary figure 1). The dry w:w ratio of CPT:PCL was 12. The electron microscopic images showed pseudo-NR aggregates because the samples were prepared by drop casting and drying of an NR suspension on a TEM grid. Moreover, samples were dried under vacuum and imaged in a high vacuum chamber that created aggregated patches of samples at the perimeter of the dried droplet. To eliminate the unambiguous NR aggregation behavior, surface charges on NRs were examined using the zeta potential. Strong negative zeta potentials of CPT NRs and CPT–PCL NRs as measured -26.8 ± 7.71 mV (online supplementary figure 2(a)) and -15.5 ± 3 mV (online supplementary figure 2(b)) in PBS, respectively indicated that the NRs were free from aggregates in colloidal dispersion. An increase in zeta potential for CPT–PCL NRs indicates the deposition of polymer on the surface of CPT NRs.

Degradation of PCL coating using FT-IR spectroscopy

The degradation of functional groups of PCL coating was determined by FT-IR analysis (figure 2). The infrared spectra of CPT–PCL NRs were compared before ($t = 0$; figure 2, dotted line) and after ($t = 72$ h; figure 2, solid line) incubation in PBS at pH 6 that mimics the slightly acidic cancer microenvironment. The presence of a strong band at 1746 cm^{-1} is due to the presence of ester carbonyl group that corresponds to the –CO stretching in PCL polymer coating before degradation (dotted line). The band intensity at 1746 cm^{-1} decreased after 72 h due to hydrolytic cleavage of ester bonds at pH 6 (solid line). The peak at 1288 cm^{-1} represents C=O stretching in the PCL polymer backbone [42], which decreases in intensity at $t = 72$ h. The peaks at 1460, 2860 and 2930 cm^{-1} correspond to the characteristic absorption of the C–H stretching bonds of ε-CL. The appearance of the peak at 2370 cm^{-1} in $t = 72$ h spectra are characteristics of –OH functional group in the carboxylic acid (–COOH) indicating the hydrolysis of ester bonds (online supplementary figure 3). The peak at 3420 cm^{-1} indicates the presence of O–H stretching in alcohol that increases in intensity at $t = 72$ h. The absorption band of the hydroxyl group is also present at $t = 0$ h, which, may be, due to absorption of moisture from the atmosphere. This also resulted in substantial artifacts in the FT-IR spectra of uncoated NRs. The FT-IR spectra of CPT NRs without PCL coating (figure 2, dash line) shows carbonyl stretching for
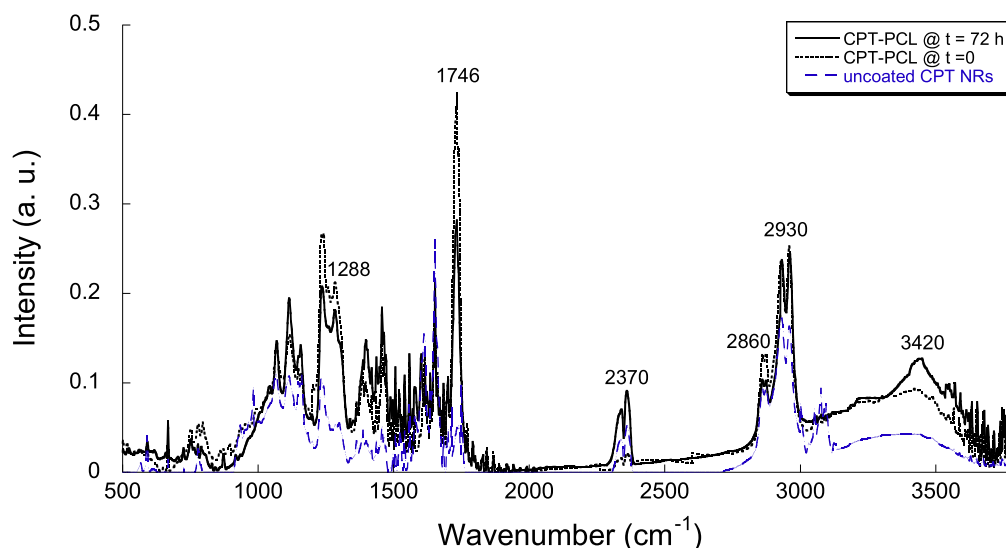
Figure 2. FT-IR graphs of CPT–PCL NRs at $t = 0$ (dotted line), $t = 72$ h (solid line) and CPT NRs without any coating (dashed line).
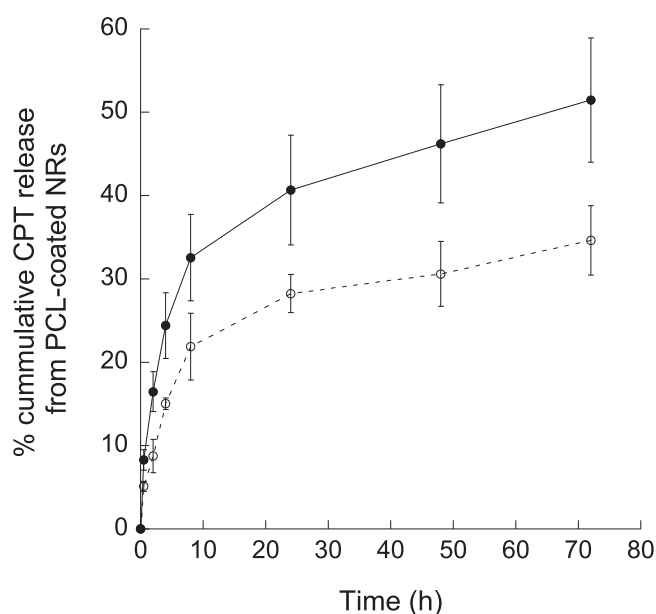

Figure 3. Cumulative percentage of CPT drug release from CPT–PCL NRs in PBS buffer at pH 6 (solid line, solid points) and pH 7.4 (dotted line, open points), and at 37 °C versus time.

cyclic ester (lactone) at $1630 \, \text{cm}^{-1}$ and C–C(=O)–O stretching for carboxylate at $1294 \, \text{cm}^{-1}$ [43]. The carboxylate peak was not observed in CPT–PCL NRs suggesting the protection of the active form of lactone rings underlying the PCL coating.

CPT drug release with PCL coating degradation

The percentage of CPT release at different time intervals is shown in figure 3 as calculated using the CPT standard curve (online supplementary figure 4). A slow release was observed at pH 6 (solid line) with 8.2% CPT release in the first 0.5 h following 32.6% release after 8 h, and 51.5% after 72 h. The release rate is comparable with the release patterns of CPT from poly(D,L-lactide-co-glycolic acid) (PLGA)

microspheres [44], and HCPT-1 from PCLLA-PEG-PCLLA [33]. At pH 7.4 (dotted line), the release profile was slower, and it needs almost 72 h to reach ~30% release, indicating the coating effect of bioresponsive PCL barrier. The influence of PCL coating on a controlled CPT release was further confirmed by faster drug release rates (~30% by 10 h) from bare CPT NRs without the PCL coating at pH 7.4 (online supplementary figure 5; solid squares; solid line). Interestingly, a decrease in the pH to 6.0 demonstrated only ~10% drug release from bare CPT NRs (online supplementary figure 5; open squares; dotted line) indicating an influence of the acid responsive PCL polymer on CPT release. The CPT drug release data were fitted to the following well-known power-law equation (3) [45, 46] to describe its release behavior from PCL polymer:
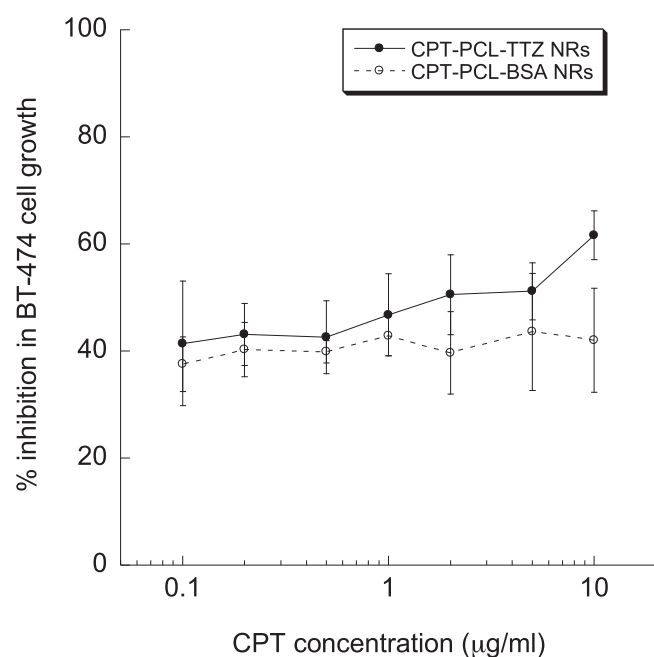
$$\frac{M_t}{M_\infty} = kt^n, \tag{3}$$

where, $\frac{M_t}{M_\infty}$ is the fraction of CPT released at the time, t, k is the kinetic constant, and n is the diffusion exponent for drug release. By plotting $\log\left(\frac{M_t}{M_\infty}\right)$ *versus* $\log t$ (online supplementary figure 6), n was calculated 0.4 for CPT drug release, indicating a Fickian drug diffusion [45, 46].

Preparation of antibody-targeted CPT–PCL–TTZ NRs

TTZ antibody was conjugated on the surface of CPT–PCL NRs by amide bond formation between the ester groups of polymer and amines on the antibody (online supplementary figure 7). The advantage of this method is the avoidance of preliminary modifications of the antibody such as activation by carbodiimide that reduces its activity [47]. TTZ covalent binding will help to deliver the NRs at breast cancer cells. The encapsulation efficiency was expressed as the weight ratio among CPT, PCL and proteins (TTZ or BSA) incorporated in NRs (table 1). The protein concentrations were measured using the BCA protein assay and BSA standard curve (online supplementary figure 8). The weight ratio of CPT:PCL:TTZ

Table 1. (a): Characterization of CPT–PCL–TTZ and CPT–PCL–BSA NR conjugates. (b): Encapsulation efficiency for CPT, PCL, TTZ and BSA in NR forms.

(a)

Amount of CPT in CPT–PCL–TTZ NRs, mg	PCL in CPT–PCL–TTZ NRs, mg	TTZ in CPT–PCL–TTZ NRs, mg	CPT:PCL:TTZ w:w ratio	CPT in CPT–PCL–BSA NRs, mg	PCL in CPT–PCL–BSA NRs, mg	BSA in CPT–PCL–BSA NRs, mg	CPT:PCL:BSA w:w ratio
4.8 ± 1.3	0.4 ± 0.05	3.7 ± 1.6	12:1:9	5 ± 0.8	0.36 ± 0.09	3.4 ± 1.7	13.9:1:9.4

(b)

	CPT	PCL	TTZ	BSA
% encapsulation/ conjugation efficiency	49.2 ± 1.1	39.9 ± 5.9	41.1 ± 1.8	33.7 ± 1.8

Figure 4. Growth inhibition curves of HER-2 positive BT-474 cells as determined by calcein-AM live-dead assay after 72 h incubation. Results are expressed as a percentage of PBS-treated control cells *versus* doses of CPT in CPT–PCL–TTZ NRs. The data represent average and standard deviation of ten treatments in three independent experiments.

and CPT:PCL:BSA were calculated as 12:1:9 and 13.9:1:9.4, respectively (table 1(a)). Table 1(b) shows the percentage encapsulation of CPT, PCL, TTZ and BSA in respective NRs.

Inhibition of breast cancer cell growth by CPT–PCL–TTZ NRs

The therapeutic activity of CPT–PCL–TTZ NRs was evaluated in HER-2 positive BT-474 (figure 4) and HER-2 negative MDA-MB-231 cells (online supplementary figure 9) at varying concentrations. The x-axes in figure 4 and online supplementary figure 9 represent the concentrations of CPT NRs where PCL and TTZ concentrations also vary at the same ratios as shown in table 1(a). The concentrations are

similar to the previously reported doses in human breast cancer cells [7, 8, 29, 48]. Cytotoxic effects by bare CPT NRs, TTZ solution alone, and PCL alone are shown in online supplementary figure 10. CPT NRs inhibited the growth of HER-2 positive BT-474 cells in a dose-dependent manner. The combination of CPT and TTZ using CPT–PCL–TTZ NRs inhibited up to 61.6% BT-474 cell growth at 10 μg ml^{-1}. At this concentration, CPT–PCL–TTZ NRs inhibited the cell growth 1.5 fold more than CPT–PCL–BSA NRs. The difference in growth inhibition between CPT–PCL–TTZ and CPT–PCL–BSA indicates the antibody dependent growth inhibition effects of TTZ on HER-2 positive BT-474 cells [49, 50]. The synergistic effect of CPT and TTZ was verified by calculating CI using equation (2). The CI was calculated $0.5 < 1.0$ using CPT NR and TTZ concentrations of 10 μg ml^{-1} and ~37 μg ml^{-1}, respectively in CPT–PCL–TTZ NRs, and the individual concentration of CPT and TTZ of 20 μg ml^{-1} and 1000 μg ml^{-1}, respectively to inhibit the same ~55% cell growth (online supplementary figures 10(a) and (b)). This indicates 2–27 fold decrease in CPT and TTZ concentrations using NRs. PCL alone without any CPT exhibited minimal (~10%) cell death both in BT-474, and MDA-MB-231 cells (online supplementary figure 10(c)) indicating that the therapeutic efficiency primarily depends on CPT and TTZ. Surprisingly the HER-2 negative MDA-MB-231 cell line was also sensitive to the NRs (online supplementary figure 8). No difference between CPT–PCL–BSA and CPT–PCL–TTZ was found in these cells, indicating non-specific CPT-evoked growth inhibition. Despite the effectiveness of active targeting of CPT–PCL–TTZ in BT-474 cells *in vitro*, we examined the intracellular uptake of the NRs. Confocal microscopic images (figure 5) showed the effective delivery of TTZ (red) conjugated CPT NRs (blue) and their colocalization (magenta) inside live BT-474 cells, indicating that the site of action for drugs was inside the cytoplasm while minimizing undesirable extracellular side effects. The colocalization of TTZ was observed across the red plasma membrane of an individual BT-474 cell. No nanoparticles were found outside of the cells.
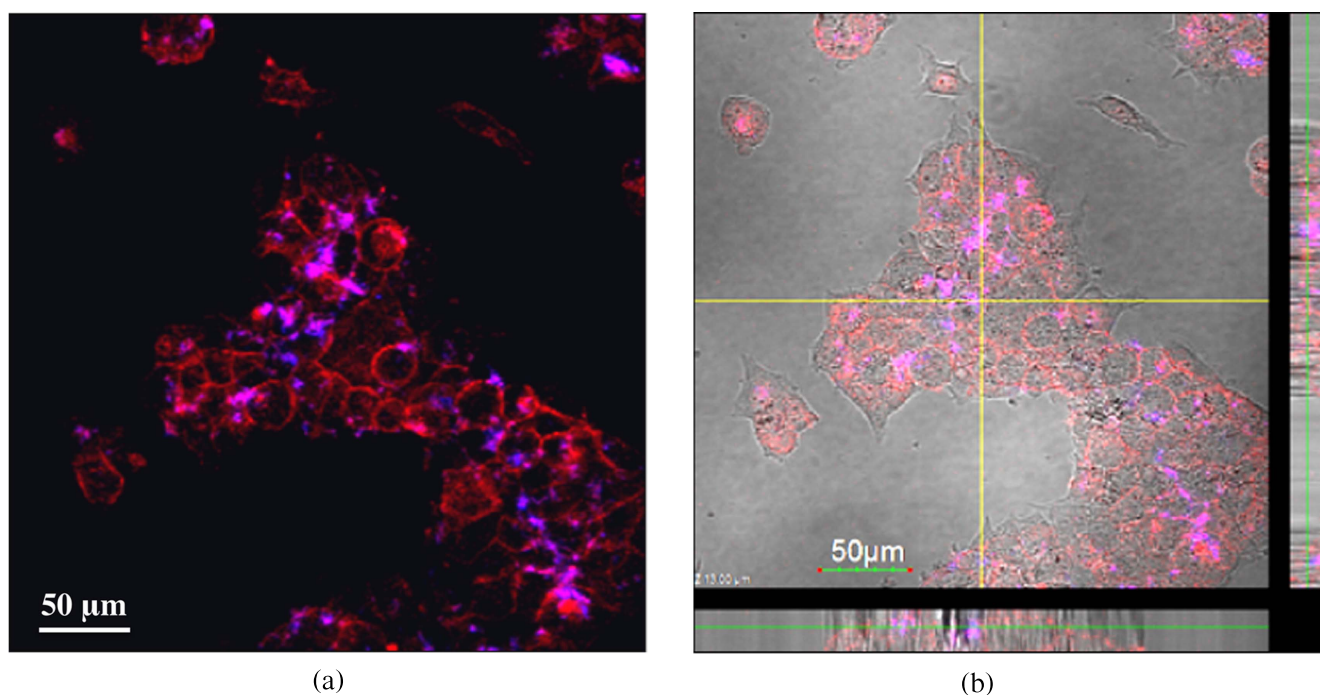
(a)   (b)

Figure 5. Confocal images of BT-474 cells treated with CPT–PCL–TTZ NRs for 6 h (a) without and (b) with a brightfield channel. Blue: CPT is intrinsically intensely fluorescent in the blue region; and red: Alexa Fluor 594 labeled TTZ. Most TTZ are mainly on the cell membrane after dissociating from NRs. The NRs are taken up by BT-474 cells. Intracellular NRs are seen in intersecting planes passing the middle of the image (b) in orthogonal *xz* (bottom) and *yz* (vertical) views. This indicates that the therapeutic effects of CPT and TTZ are exerted intracellularly. Scale bar = 50 μm.

Discussion

The study of PCL polymers for CPT NR coating reveals protection of the drug *in vitro*. At physiological pH, the unstable E-ring lactone in CPT is converted to carboxylate form, which possesses high affinity to HSA and is preferentially eliminated [1, 2]. This is a clinical hurdle to CPT therapeutic efficiency. Encapsulation of CPT inside PCL polymer coating prevents CPT from being converted into the inactive carboxylate form [51, 52]. As it is observed from the FT-IR data (figure 2) that the PCL coating undergoes hydrolytic degradation producing non-toxic by-products (alcohol and water) (online supplementary figure 3). The slow degradation of the polymers released CPT drugs from NRs at pH 6 (figure 3; solid line). At pH 7.4, PCL polymer coating does not allow for fast CPT penetration (figure 3; dotted line).

The elongated NR design allows for long circulation time in the body [24, 26, 53–55], and multivalent interactions with cancer cells [21, 56, 57], increasing the probability of receptor-ligand interactions. It is shown that the active targeting of breast cancer cells using the similar dimension of NRs of CPT with TTZ attached to the breast cancer cell surface [18, 29]. The layer of TTZ antibody on the surface of NRs offers the feature of targeted therapy.

We simulated the acidic nature of cancer cell microenvironment [58, 59] using PBS at pH 6 and determined the effects on the stability of NRs. The *in vitro* release of CPT in the first 30 min was minimal, with only 7.4% of the total CPT drugs in NRs being released (figure 3; solid line). The

polymer coating began to disintegrate, releasing ∼40% of total CPT in 24 h and more than 50.8% in 72 h. A 100% drug release of CPT was limited by its low (∼10 μg ml^{-1}) water solubility [60, 61]. Galbiate *et al* measured 40% cumulative dissolution of CPT over 3 days from chitosan biopolymer coated microcapsules in PBS of pH 7.4 [62]. Approx. 20% CPT release from polydopamine nanoparticles had been reported over a period of 24 h at pH 7.5 [63]. The *in vitro* data provide guidance for understanding the fundamentals of CPT drug release, however, burst release of drugs may occur under complex physiological conditions such as high fluid pressures, and the presence of enzymes.

Interaction with cancer cells is important for most nanoparticles reaching the target site. We performed molecular targeting by conjugating TTZ to the surface of CPT–PCL NRs. It was observed that the HER-2 negative MDA-MB-231 cell line was also sensitive to NRs (online supplementary figure 9). No difference between CPT–PCL–BSA and CPT–PCL–TTZ was found in these cells. We conjecture that this might be due to effective non-specific endocytosis *in vitro*. Collectively, our results support a purely cytostatic effect of these drugs *in vitro*.

Conclusions

We have developed a simple method of a thin (10.3 ± 1.4 nm) layer of bioresponsive PCL polymer coating on CPT anti-cancer drug NRs. As the drug molecules

precipitated out of its organic solvent into an aqueous phase, the molecules aggregated and formed NRs. The PCL polymers spread thinly over drug NRs due to van der Waals and hydrogen bonding effects. This process did not produce any adverse mechanical effects to prepare the NRs, thereby, retaining active structures of therapeutic drugs. One merit of our method is the preparation of PCL-coated CPT NRs of $(500.9 \pm 91.3 \times 122.7 \pm 10.1)$ nm size in large quantities. We characterized the degradation of CPT–PCL NRs using FT-IR analysis, and release of CPT in a simulated pH condition in cancer microenvironment. Conjugation of TTZ to the surface of CPT–PCL NRs significantly inhibited the growth of BT-474 breast cancer cells. Overexpression of HER-2 increases breast cancer cell proliferation in part by transactivation of enhanced growth factor receptor signaling [37, 49, 64]. Blocking of HER-2 by TTZ binding proved to suppress the cells growth. *In vivo* studies are needed for therapeutic efficacy. Nonetheless, our current results found thus far are promising and continue to shed the light of inherent benefits of improved breast cancer therapy.

Acknowledgments

References

[1] Jaxel C, Capranico G, Kerrigan D, Kohn K W and Pommier Y 1991 Effect of local DNA sequence on topoisomerase I cleavage in the presence or absence of camptothecin *J. Biol. Chem.* **266** 20418 https://www.ncbi.nlm.nih.gov/pubmed/1657924

[2] Jaxel C, Kohn K W, Wani M C, Wall M E and Pommier Y 1989 Structure-activity study of the actions of camptothecin derivatives on mammalian topoisomerase: I. evidence for a specific receptor site and a relation to antitumor activity *Cancer Res.* **49** 1465–9 https://www.ncbi.nlm.nih.gov/pubmed/2538227

[3] Svenson S, Wolfgang M, Hwang J, Ryan J and Eliasof S 2011 Preclinical to clinical development of the novel camptothecin nanopharmaceutical CRLX101 *J. Control. Rel.* **153** 49–55

[4] Homsi J *et al* 2007 Phase I trial of poly-l-glutamate camptothecin (CT-2106) administered weekly in patients with advanced solid malignancies *Clin. Cancer Res.* **13** 5855–61

[5] Han H and Davis M E 2013 Single-antibody, targeted nanoparticle delivery of camptothecin *Mol. Pharmaceutics* **10** 2558–67

[6] Schluep T, Hwang J, Cheng J, Heidel J D, Bartlett D W, Hollister B and Davis M E 2006 Preclinical efficacy of the camptothecin–polymer conjugate IT-101 in multiple cancer models *Clin. Cancer Res.* **12** 1606–14

[7] Cheng J, Khin K T, Jensen G S, Liu A and Davis M E 2003 Synthesis of linear, *β*-cyclodextrin-based polymers and their camptothecin conjugates *Bioconjugate Chem.* **14** 1007–17

[8] Cheng J, Khin K T and Davis M E 2004 Antitumor activity of beta-cyclodextrin polymer-camptothecin conjugates *Mol. Pharm.* **1** 183–93

[9] Bissett D *et al* 2004 Phase I and pharmacokinetic (PK) study of MAG-CPT (PNU 166148): a polymeric derivative of camptothecin (CPT) *Br. J. Cancer* **91** 50–5

[10] Oledzka E, Horeglad P, Gruszczyńska Z, Plichta A, Nałęcz-Jawecki G and Sobczak M 2014 Polylactide conjugates of camptothecin with different drug release abilities *Molecules* **19** 19460

[11] Chen X, McRae S, Parelkar S and Emrick T 2009 Polymeric phosphorylcholine−camptothecin conjugates prepared by controlled free radical polymerization and click chemistry *Bioconjugate Chem.* **20** 2331–41

[12] Batist G, Gelmon K A, Chi K N, Miller W H, Chia S K L, Mayer L D, Swenson C E, Janoff A S and Louie A C 2009 Safety, pharmacokinetics, and efficacy of CPX-1 liposome injection in patients with advanced solid tumors *Clin. Cancer Res.* **15** 692–700

[13] Yanagihara K, Takigahira M, Kubo T, Ochiya T, Hamaguchi T and Matsumura Y 2014 Marked antitumor effect of NK012, a SN-38-incorporating micelle formulation, in a newly developed mouse model of liver metastasis resulting from gastric cancer *Therapeutic Deliv.* **5** 129–38

[14] Bissett D *et al* 2004 Phase I and pharmacokinetic (PK) study of MAG-CPT (PNU 166148): a polymeric derivative of camptothecin (CPT) *Br. J. Cancer* **91** 50–5

[15] Yurkovetskiy A V and Fram R J 2009 XMT-1001, a novel polymeric camptothecin pro-drug in clinical development for patients with advanced cancer *Adv. Drug. Deliv. Rev.* **61** 1193–202

[16] Coelho J F, Ferreira P C, Alves P, Cordeiro R, Fonseca A C, Góis J R and Gil M H 2010 Drug delivery systems: advanced technologies potentially applicable in personalized treatments *EPMA J.* **1** 164–209

[17] Yan G, Paul D, Shenshen C, Richard T, Manorama T, Tamara M and Dennis E D 2007 Shape effects of filaments versus spherical particles in flow and drug delivery *Nat. Nanotechnol.* **2** 249–55

[18] Barua S, Yoo J-W, Kolhar P, Wakankar A, Gokarn Y R and Mitragotri S 2013 Particle shape enhances specificity of antibody-displaying nanoparticles *Proc. Natl Acad. Sci.* **110** 3270–5

[19] Decuzzi P and Ferrari M 2006 The adhesive strength of non-spherical particles mediated by specific interactions *Biomaterials* **27** 5307–14

[20] Decuzzi P and Ferrari M 2008 The receptor-mediated endocytosis of nonspherical particles *Biophys. J.* **94** 3790–7

[21] Gratton S E A, Ropp P A, Pohlhaus P D, Luft J C, Madden V J, Napier M E and DeSimone J M 2008 The effect of particle design on cellular internalization pathways *Proc. Natl Acad. Sci.* **105** 11613–8

[22] Huang X, Teng X, Chen D, Tang F and He J 2010 The effect of the shape of mesoporous silica nanoparticles on cellular uptake and cell function *Biomaterials* **31** 438–48

[23] Champion J A and Mitragotri S 2006 Role of target geometry in phagocytosis *Proc. Natl Acad. Sci. USA* **103** 4930–4

[24] Muro S, Garnacho C, Champion J A, Leferovich J, Gajewski C, Schuchman E H, Mitragotri S and

Muzykantov V R 2008 Control of endothelial targeting and intracellular delivery of therapeutic enzymes by modulating the size and shape of ICAM-1-targeted carriers *Mol. Ther.* **16** 1450–8

[25] Gentile F, Chiappini C, Fine D, Bhavane R C, Peluccio M S, Cheng M M-C, Liu X, Ferrari M and Decuzzi P 2008 The effect of shape on the margination dynamics of non-neutrally buoyant particles in two-dimensional shear flows *J. Biomech.* **41** 2312–8

[26] Decuzzi P, Godin B, Tanaka T, Lee S Y, Chiappini C, Liu X and Ferrari M 2010 Size and shape effects in the biodistribution of intravascularly injected particles *J. Control. Rel.* **141** 320–7

[27] Adriani G, de Tullio M D, Ferrari M, Hussain F, Pascazio G, Liu X and Decuzzi P 2012 The preferential targeting of the diseased microvasculature by disk-like particles *Biomaterials* **33** 5504–13

[28] Godin B, Chiappini C, Srinivasan S, Alexander J F, Yokoi K, Ferrari M, Decuzzi P and Liu X 2012 Drug delivery: discoidal porous silicon particles: fabrication and biodistribution in breast cancer bearing mice *Adv. Funct. Mater.* **22** 4186–4186

[29] Barua S and Mitragotri S 2013 Synergistic targeting of cell membrane, cytoplasm, and nucleus of cancer cells using rod-shaped nanoparticles *ACS Nano* **7** 9558–70

[30] Woodruff M A and Hutmacher D W 2010 The return of a forgotten polymer—polycaprolactone in the 21st century *Prog. Polym. Sci.* **35** 1217–56

[31] Kumari A, Yadav S K and Yadav S C 2010 Biodegradable polymeric nanoparticles based drug delivery systems *Colloids Surf.* B **75** 1–18

[32] Yang Y-Y, Chung T-S and Ng P N 2001 Morphology, drug distribution, and *in vitro* release profiles of biodegradable polymeric microspheres containing protein fabricated by double-emulsion solvent extraction/evaporation method *Biomaterials* **22** 231–41

[33] Zhang L, Yang M, Wang Q, Li Y, Guo R, Jiang X, Yang C and Liu B 2007 10-hydroxycamptothecin loaded nanoparticles: preparation and antitumor activity in mice *J. Control. Rel.* **119** 153–62

[34] Kang Y M, Kim G H, Kim J I, Kim D Y, Lee B N, Yoon S M, Kim J H and Kim M S 2011 *In vivo* efficacy of an intratumorally injected *in situ*-forming doxorubicin/poly (ethylene glycol)-b-polycaprolactone diblock copolymer *Biomaterials* **32** 4556–64

[35] Gao H, Wang Y N, Fan Y G and Ma J B 2005 Synthesis of a biodegradable tadpole-shaped polymer via the coupling reaction of polylactide onto mono(6-(2-aminoethyl)amino-6-deoxy)-β-cyclodextrin and its properties as the new carrier of protein delivery system *J. Control. Rel.* **107** 158–73

[36] Barua S, Yoo J W, Kolhar P, Wakankar A, Gokarn Y R and Mitragotri S 2013 Particle shape enhances specificity of antibody-displaying nanoparticles *Proc. Natl Acad. Sci. USA* **110** 3270–5

[37] Boekhout A H, Beijnen J H and Schellens J H M 2011 Trastuzumab *Oncologist* **16** 800–10

[38] Dean-Colomb W and Esteva F J 2008 Her2-positive breast cancer: herceptin and beyond *Eur. J. Cancer* **44** 2806–12

[39] Chou T-C 2010 Drug combination studies and their synergy quantification using the Chou–Talalay method *Cancer Res.* **70** 440–6

[40] Chou T-C and Talalay P 1984 Quantitative analysis of dose-effect relationships: the combined effects of multiple drugs or enzyme inhibitors *Adv. Enzyme Regul.* **22** 27–55

[41] Chen E-C and Wu T-M 2007 Isothermal crystallization kinetics and thermal behavior of poly(ε-caprolactone)/multi-walled carbon nanotube composites *Polym. Degrad. Stab.* **92** 1009–15

[42] Elzein T, Nasser-Eddine M, Delaite C, Bistac S and Dumas P 2004 FTIR study of polycaprolactone chain organization at interfaces *J. Colloid Interface Sci.* **273** 381–7

[43] Tong W, Wang L and D'Souza M J 2003 Evaluation of PLGA microspheres as delivery system for antitumor agent-camptothecin *Drug Dev. Ind. Pharmacy* **29** 745–56

[44] Ertl B, Platzer P, Wirth M and Gabor F 1999 Poly(D,L-lactic-co-glycolic acid) microspheres for sustained delivery and stabilization of camptothecin *J. Control. Rel.* **61** 305–17

[45] Korsmeyer R W, Gurny R, Doelker E, Buri P and Peppas N A 1983 Mechanisms of solute release from porous hydrophilic polymers *Int. J. Pharmaceutics* **15** 25–35

[46] Peppas N A 1985 Analysis of Fickian and non-Fickian drug release from polymers *Pharm. Acta Helv.* **60** 110–1 https://www.ncbi.nlm.nih.gov/pubmed/4011621

[47] Kocbek P, Obermajer N, Cegnar M, Kos J and Kristl J 2007 Targeting cancer cells using PLGA nanoparticles surface modified with monoclonal antibody *J. Control. Rel.* **120** 18–26

[48] Cirpanli Y, Bilensoy E, Dogan A L and Calis S 2010 Development of polymeric and cyclodextrin nanoparticles for camptothecin delivery *J. Control. Rel.* **148** e21–3

[49] Sadeghi S, Olevsky O and Hurvitz S A 2014 Profiling and targeting HER2-positive breast cancer using trastuzumab emtansine *Pharmacogenomics Personalized Med.* **7** 329–38

[50] Lewis Phillips G D *et al* 2008 Targeting HER2-Positive breast cancer with trastuzumab-DM1, an antibody–cytotoxic drug conjugate *Cancer Res.* **68** 9280–90

[51] Huang Y-Y, Chung T-W and Tzeng T-W 1999 A method using biodegradable polylactides/polyethylene glycol for drug release with reduced initial burst *Int. J. Pharmaceutics* **182** 93–100

[52] Xue M, Hu H, Jiang Y, Liu J, He H and Ye X 2012 Biodegradable polymer-coated, gelatin hydrogel/bioceramics ternary composites for antitubercular drug delivery and tissue regeneration *J. Nanomater.* **2012** 8

[53] Geng Y, Dalhaimer P, Cai S, Tsai R, Tewari M, Minko T and Discher D E 2007 Shape effects of filaments versus spherical particles in flow and drug delivery *Nat. Nano* **2** 249–55

[54] Kolhar P, Anselmo A C, Gupta V, Pant K, Prabhakarpandian B, Ruoslahti E and Mitragotri S 2013 Using shape effects to target antibody-coated nanoparticles to lung and brain endothelium *Proc. Natl Acad. Sci.* **110** 10753–8

[55] Liu Y, Tan J, Thomas A, Ou-Yang D and Muzykantov V R 2012 The shape of things to come: importance of design in nanotechnology for drug delivery *Therapeutic Deliv.* **3** 181–94

[56] Perry J L, Herlihy K P, Napier M E and DeSimone J M 2011 PRINT: a novel platform toward shape and size specific nanoparticle theranostics *Acc. Chem. Res.* **44** 990–8

[57] Fromen C A, Robbins G R, Shen T W, Kai M P, Ting J P Y and DeSimone J M 2015 Controlled analysis of nanoparticle charge on mucosal and systemic antibody responses following pulmonary immunization *Proc. Natl Acad. Sci.* **112** 488–93

[58] Tannock I F and Rotin D 1989 Acid pH in tumors and its potential for therapeutic exploitation *Cancer Res.* **49** 4373–84 https://www.ncbi.nlm.nih.gov/pubmed/2545340

[59] Kato Y, Ozawa S, Miyamoto C, Maehata Y, Suzuki A, Maeda T and Baba Y 2013 Acidic extracellular microenvironment and cancer *Cancer Cell Int.* **13** 89–89

[60] Wall M E, Wani M C, Cook C E, Palmer K H, McPhail A T and Sim G A 1966 Plant antitumor agents: I. The isolation and structure of camptothecin, a novel alkaloidal leukemia and tumor inhibitor from *Camptotheca acuminata J. Am. Chem. Soc.* **88** 3888–90

[61] Nalluri B N, Devineni P K, Male M K, Shaik A S and Uppuluri C T 2015 Studies on development of controlled

release matrix tablets of camptothecin—an anticancer drug *Indian J. Pharmaceutical Edu. Res.* **49** 292–300

[62] Galbiati A, Rocca B M D, Tabolacci C, Beninati S, Desideri A and Paradossi G 2011 PVA engineered microcapsules for targeted delivery of camptothecin to HeLa cells *Mater. Sci. Eng.* C **31** 1653–9

[63] Ho C-C and Ding S-J 2013 The pH-controlled nanoparticles size of polydopamine for anti-cancer drug delivery *J. Mater. Sci., Mater. Med.* **24** 2381–90

[64] Bullock K and Blackwell K 2008 Clinical efficacy of taxane– trastuzumab combination regimens for HER-2–positive metastatic breast cancer *Oncologist* **13** 515–25